VU VRIJE UNIVERSITEIT AMSTERDAM

VU Research Portal

Reactive and diffractive scattering of H-2 from Pt(111) studied using a six-dimensional wave packet method

Pijper, E.; Kroes, G.; Olsen, R.A.; Baerends, E.J.

published in
Journal of Chemical Physics
2002

DOI (link to publisher)
10.1063/1.1501121

document version
Publisher's PDF, also known as Version of record

Link to publication in VU Research Portal

citation for published version (APA)
Pijper, E., Kroes, G., Olsen, R. A., & Baerends, E. J. (2002). Reactive and diffractive scattering of H-2 from Pt(111) studied using a six-dimensional wave packet method. *Journal of Chemical Physics*, *117*(12), 5885-5898. https://doi.org/10.1063/1.1501121

General rights
Copyright and moral rights for the publications made accessible in the public portal are retained by the authors and/or other copyright owners and it is a condition of accessing publications that users recognise and abide by the legal requirements associated with these rights.

- Users may download and print one copy of any publication from the public portal for the purpose of private study or research.
- You may not further distribute the material or use it for any profit-making activity or commercial gain
- You may freely distribute the URL identifying the publication in the public portal ?

Take down policy
If you believe that this document breaches copyright please contact us providing details, and we will remove access to the work immediately and investigate your claim.

E-mail address:
vuresearchportal.ub@vu.nl

Download date: 26. Sep. 2021

Reactive and diffractive scattering of H_2 from Pt(111) studied using a six-dimensional wave packet method

E. Pijper and G. J. Kroes
Leiden Institute of Chemistry, Gorlaeus Laboratories, Leiden University, P.O. Box 9502, 2300 RA Leiden, The Netherlands

R. A. Olsen and E. J. Baerends
Theoretische Chemie, Vrije Universiteit, De Boelelaan 1083, 1081 HV Amsterdam, The Netherlands

(Received 7 May 2002; accepted 24 June 2002)

We present results of calculations on dissociative and rotationally (in)elastic diffractive scattering of H_2 from Pt(111), treating all six molecular degrees of freedom quantum mechanically. The six-dimensional (6D) potential energy surface was taken from density functional theory calculations using the generalized gradient approximation and a slab representation of the metal surface. The 6D calculations show that out-of-plane diffraction is very efficient, at the cost of in-plane diffraction, as was the case in previous four-dimensional (4D) calculations. This could explain why so little in-plane diffraction was found in scattering experiments, suggesting the surface to be flat, whereas experiments on reaction suggested a corrugated surface. Results of calculations for off-normal incidence of $(v=0,j=0)$ H_2 show that initial parallel momentum inhibits dissociation at low normal translational energies, in agreement with experiment, but has little effect for higher energies. Reaction of initial $(v=1,j=0)$ H_2 is predicted to be vibrationally enhanced with respect to $(v=0,j=0)$ H_2, as was also found in three-dimensional (3D) and 4D calculations, even though $H_2+Pt(111)$ is an early barrier system. © *2002 American Institute of Physics.*
[DOI: 10.1063/1.1501121]

I. INTRODUCTION

This is the third paper in a series of quantum dynamics calculations on scattering of H_2 from Pt(111), which is here studied including all six molecular degrees of freedom of H_2 with respect to the metal surface. Previous studies concerned reduced two-dimensional (2D),[1] three-dimensional (3D),[1] and four-dimensional (4D) (Ref. 2) calculations. With the present six-dimensional (6D) calculations, we hope to gain insight into a problem that has motivated us from the beginning, and is related to how corrugated the potential energy surface (PES) of the $H_2+Pt(111)$ system is and what the effect is of the corrugation on reactive and diffractive scattering.

A contradiction[3] is presented by molecular beam experiments on sticking of D_2 and H_2 on Pt(111),[4] and rotationally inelastic diffraction of HD scattering from Pt(111).[5] In the former, the results showed the sticking to depend on the initial momentum of D_2 parallel to the surface, suggesting that the PES must be corrugated. The latter experiment, however, showed almost no diffraction, implying a flat PES. The paradox implied by these two experiments is an important motivation for studying the $H_2+Pt(111)$ system.

The problem of conflicting views on the amount of corrugation of the $H_2+Pt(111)$ system has also been the discussed in earlier 3D (Ref. 1) and 4D (Ref. 2) calculations. In the 3D calculations, the degrees of freedom were the center-of-mass distance to the surface *Z*, the internuclear distance *r* and one degree of freedom for motion parallel to the surface, *X*. In the 4D calculations, the 3D model was extended with a second degree of freedom for motion parallel to the surface, *Y*. In both the 3D and the 4D model, the molecular bond was kept parallel to the surface. These calculations yielded an interesting prediction: even though all barriers are early, vibrational enhancement was found nonetheless. This was unexpected because vibrational enhancement is usually associated with late barriers.[6,7] However, our analysis showed that in the entrance channel the force constant associated with the vibration decreased as the molecule approached the barrier. The vibrational energy that is released in this process can flow into translation along *Z*, thereby enhancing reaction. A similar mechanism had previously been predicted for $H_2+Pd(100)$,[8] and confirmed in recent associative desorption experiments.[9]

In both the 3D and 4D calculations, we found that normal energy scaling was not obeyed, in agreement with the experimental results of Luntz *et al.*[4] When looking at diffraction, an important difference was found between the 3D and 4D calculations. In the 3D calculations, substantial diffraction was found. Because only one degree of freedom parallel to the surface was included, all diffraction was in-plane, i.e., in the plane of incidence. In the 4D calculations, a second degree of freedom parallel to the surface was also included, and resulted in out-of-plane diffraction becoming more important than in-plane diffraction. Because Cowin *et al.*[5] only looked at in-plane diffraction, our 4D results suggested that experimental proof of a corrugated PES can be found by measuring out-of-plane diffraction, and that by only looking at in-plane diffraction an incomplete picture was presented.

In the present paper we present results of six-dimensional (6D) calculations, treating all molecular degrees

 © 2002 American Institute of Physics

Downloaded 27 Mar 2011 to 130.37.129.78. Redistribution subject to AIP license or copyright; see http://jcp.aip.org/about/rights_and_permissions

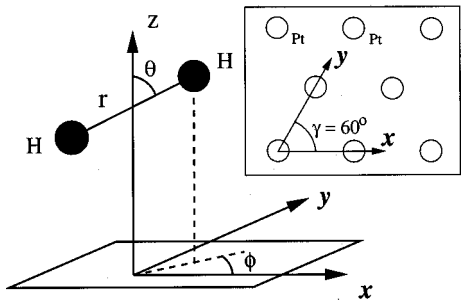

FIG. 1. The coordinate system used for describing H_2 interacting with a static Pt(111) surface. The inset shows the nonorthogonality of the x and y coordinates, which are taken along the sides of the diamond shaped unit cell. The skewing angle $\gamma = 60°$.

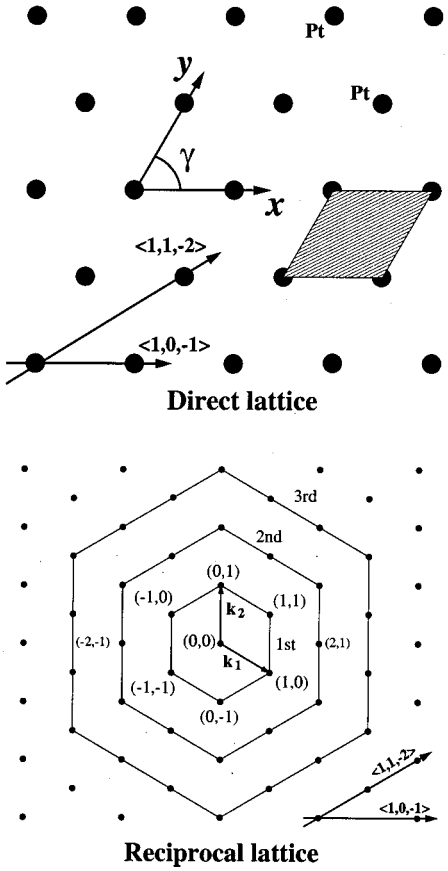

FIG. 2. The direct lattice (top figure) and reciprocal lattice (bottom figure) of the Pt(111) surface. The direct lattice shows the surface unit cell (shaded area) and the x and y coordinate axes used. The angle γ is called the skewing angle and equals 60°. Points on the reciprocal lattice correspond to diffraction states allowed during scattering. The hexagonal rings define the diffraction order. In both figures the $\langle 10\bar{1}\rangle$ and $\langle 11\bar{2}\rangle$ directions are indicated.

of freedom. Important questions concern the precise role of the rotations. Will rotational excitation occur at the expense of diffraction, leading to small diffraction probabilities as measured in experiment, or will the general picture of the 4D model still hold?

We will present results for normal and off-normal incidence, and look at the effect of corrugation on diffraction and dissociation. All degrees of freedom in the 6D model are treated quantum mechanically. The calculations are performed using the time-dependent wave packet (TDWP) method.[10] We use a 6D potential energy surface (PES) obtained from an interpolation of fourteen 2D PESs, using a corrugation reducing scheme developed by Busnengo *et al.*[11] Each 2D PES is a spline interpolation of potential points calculated with density functional theory (DFT), employing the generalized gradient approximation (GGA) (Refs. 12, 13) and using a slab representation of the surface.[14,15]

This paper is organized as follows: In Sec. II, the dynamical method and the PES we use are briefly described. In Sec. III, the results of 6D calculations are presented. In Sec. III A, reaction is discussed for normal incidence. Rotational excitation probabilities are presented in Sec. III C. Results for reaction and diffraction at off-normal incidence are presented in Secs. III B and III D, respectively. The comparison with experiment is discussed in Sec. III E for reaction and in Sec. III F for diffraction. Section IV concludes.

II. THEORY

A. 6D dynamics model

The interaction of H_2 with a Pt(111) surface is modeled six-dimensionally (6D) by treating all molecular degrees of freedom. The coordinates used to model H_2 are shown in Fig. 1. Three translational coordinates are used to describe the motion of the center-of-mass of H_2; the distance to the surface Z, and two coordinates for motion parallel to the surface, x and y. The remaining three coordinates, r, θ and ϕ, describe the H–H internuclear separation and orientation, respectively. The angle θ is the polar angle of the H–H bond with respect to the surface normal. The angle ϕ is the azimuthal angle of the projection of the H–H bond onto the surface, with respect to the x-axis.

The Born–Oppenheimer approximation is used to decouple the motion of the nuclei from the motion of the electrons, restricting (reactive) scattering to take place on the ground state potential energy surface (PES). Furthermore, the surface is treated as being static, placing the Pt atoms at their ideal lattice positions. As a consequence, energy transfer through phonon creation and/or annihilation is not possible. These two approximations are the usual approximations made in surface scattering,[16,17] although quantum dynamical reduced dimensionality calculations that include energy exchange with the surface have also been done (see, for instance, Refs. 18–21).

All six degrees of freedom of the H_2 molecule are treated quantum mechanically. The skewed nature of the surface unit cell of the Pt(111) surface suggests the use of nonorthogonal coordinates x and y (see inset of Fig. 1). Here, the x- and y-axis are taken along the sides of a diamond shaped unit cell (see Fig. 2). The 6D Hamiltonian for nuclear motion is then given by[2,22,23]

$$\hat{H} = -\frac{1}{2M}\frac{\partial}{\partial Z^2} - \frac{1}{2M\sin^2\gamma} \times\left[\frac{\partial}{\partial x^2} - 2\cos\gamma\frac{\partial}{\partial x}\frac{\partial}{\partial y} + \frac{\partial}{\partial y^2}\right] - \frac{1}{2\mu}\frac{\partial}{\partial r^2} + \frac{\hat{J}^2}{2\mu r^2} + V_{6D}(Z,r,x,y,\theta,\phi), \quad (1)$$

Downloaded 27 Mar 2011 to 130.37.129.78. Redistribution subject to AIP license or copyright; see http://jcp.aip.org/about/rights_and_permissions

where atomic units have been used. The masses M and μ are the total and reduced mass of H_2, respectively. The angle γ is the angle between the x and y coordinate axes as indicated in Fig. 2. For Pt(111), $\gamma=60°$. The cross term in Eq. (1) involving the first derivatives with respect to x and y results from the use of nonorthogonal coordinates.[22,23] The operator $\hat{j}$ is the rotation operator. Its eigenfunctions are the spherical harmonics $Y_{jm_j}(\theta,\phi)$. The 6D interaction potential is represented by V_{6D}, and described in Sec. II B.

To obtain scattering and reaction probabilities, a time-dependent wave packet (TDWP) method[10] is used. To represent the dependence of the wave function on Z, r, x, and y, we use a direct product discrete variable representation (DVR) (Ref. 24) with constant grid spacings ΔZ, Δr, Δx, and Δy. Fast Fourier transforms[25,26] are used to transform the wave function from the DVR to a direct product finite basis representation (FBR) in momentum space, and vica versa. To represent the dependence of the wave function on θ and ϕ, we use a non-direct product finite basis representation (FBR) of spherical harmonics $Y_{jm_j}(\theta,\phi)$. Gauss–Legendre and Fourier transformations are used to transform the wave function from the nondirect FBR representation to a direct product discrete variable representation in θ and ϕ,[27,28] respectively, and vice versa.

The calculation is carried out by propagating an initial wave packet (placed far from the surface where the interaction with the surface is negligible) according to the time-dependent Schrödinger equation. The back scattered part of the wave function is analyzed at a dividing surface placed at Z_∞ where the molecule and the surface no longer interact. Beyond Z_∞ an optical potential is used to absorb the wave function once it has been analyzed.[29] The reactive part of the wave function is absorbed once the internuclear distance becomes larger than some value r_d.

The wave function is analyzed using a formalism developed by Balint-Kurti *et al.*[30–32] State-to-state scattering probabilities $P(v,j,m_j\rightarrow v',j',m_j',n,m)$ are obtained for the energy range contained in the initial wave packet. The reaction probability as a function of the collision energy E_i is then computed by summing over all state-to-state probabilities for E_i, and then subtracting the sum from 1.

The propagation is carried our using the split operator (SPO) method,[25] in which the kinetic and potential propagation part of the Hamiltonian are symmetrically split according to

$$\begin{aligned}\exp(-i\hat{H}\Delta t)=&\exp(-i\hat{K}\Delta t/2)\times\exp(-i\hat{j}^2/(2\mu r^2)\Delta t/2)\\&\times\exp(-i\hat{V}\Delta t)\times\exp(-i\hat{j}^2/(2\mu r^2)\Delta t/2)\\&\times\exp(-i\hat{K}\Delta t/2).\end{aligned}\tag{2}$$

By symmetrizing the splitting, the error in the SPO is of the order Δt^3.

The treatment of the skewed nature of the surface unit cell of Pt(111) is facilitated by the use of nonorthogonal coordinates x and y. In Ref. 2, the use of nonorthogonal coordinates to describe motion parallel to the surface, and the connection with the individual diffraction states, is extensively described for a general skewed unit cell. Figure 2 shows the direct and reciprocal lattice of the Pt(111) surface. The unit cell of the Pt(111) surface is indicated by the shaded area in the direct lattice. Also indicated are the nonorthogonal x- and y-axis. The points on the reciprocal lattice (with respect to a chosen origin) correspond to diffraction states in which momentum parallel to the surface has been gained or lost.

In discussing the results, we will often use the concept of diffraction order. For the (111) surface of Pt, diffraction order is defined by drawing hexagonal rings around a chosen origin that refers to specular scattering. Diffraction states on the same hexagonal ring are asigned the same diffraction order, counting outwards and starting with 0 for the (0,0) specular state.[2]

B. PES

To construct a six-dimensional potential energy surface (PES), density functional theory (DFT) calculations were done for H+Pt(111) and H_2+Pt(111). The DFT calculations were performed with the program BAND,[14] employing the generalized gradient approximation (GGA).[12,13] The surface was modeled by a 3 layers slab representation[14,15] using a 2×2 surface unit cell.[33] Relativistic effects were accounted for by the zero-order regular approximation (ZORA).[34]

The 6D PES (Ref. 35) was constructed from a number of 2D PESs in Z and r. Each 2D PES is a spline interpolation of 50–60 points calculated with DFT. A major task was to interpolate the 2D PESs to form a 6D PES that accurately represents the potential over the entire six-dimensional coordinate space. Due to the strong corrugation near the surface, a straightforward interpolation can lead to large deviations and artefacts in this region[1] for points x, y, θ, and ϕ not calculated with DFT. Busnengo *et al.*[11] developed a "corrugation reducing procedure" that reduces the strong corrugation near the surface by subtracting the H–surface interaction from the H_2–surface interaction, leaving a set of reduced "2D PESs" that are much smoother and therefore more easily interpolated accurately. The H-surface potential is then added back to the interpolated potential,

$$\begin{aligned}V_{6D}(x,y,Z,r,\theta,\phi)=&I_{6D}(x,y,Z,r,\theta,\phi)\\&+V_{3D}(X_A,Y_A,Z_A)\\&+V_{3D}(X_B,Y_B,Z_B),\end{aligned}\tag{3}$$

where (X_A,Y_A,Z_A) and (X_B,Y_B,Z_B) refer to the coordinates of atom A and B, respectively. In Eq. (3), $I_{6D}(x,y,Z,r,\theta,\phi)$ represents the interpolated set of reduced 2D PESs. The potentials, $V_{3D}(X_A,Y_A,Z_A)$ and $V_{3D}(X_B,Y_B,Z_B)$ are the interpolated 3D potentials for atoms A and B, respectively. They are obtained by also applying the corrugation reducing procedure to the H-surface potential.[11] More details concerning the interpolation can be found in Refs. 11 and 35.

The accuracy of the 6D potential was tested by performing DFT calculations for various points not included in the interpolation data set and comparing them with the interpolated values. The comparison showed that the maximum error is 30 meV for both the entrance channel and barrier

Downloaded 27 Mar 2011 to 130.37.129.78. Redistribution subject to AIP license or copyright; see http://jcp.aip.org/about/rights_and_permissions

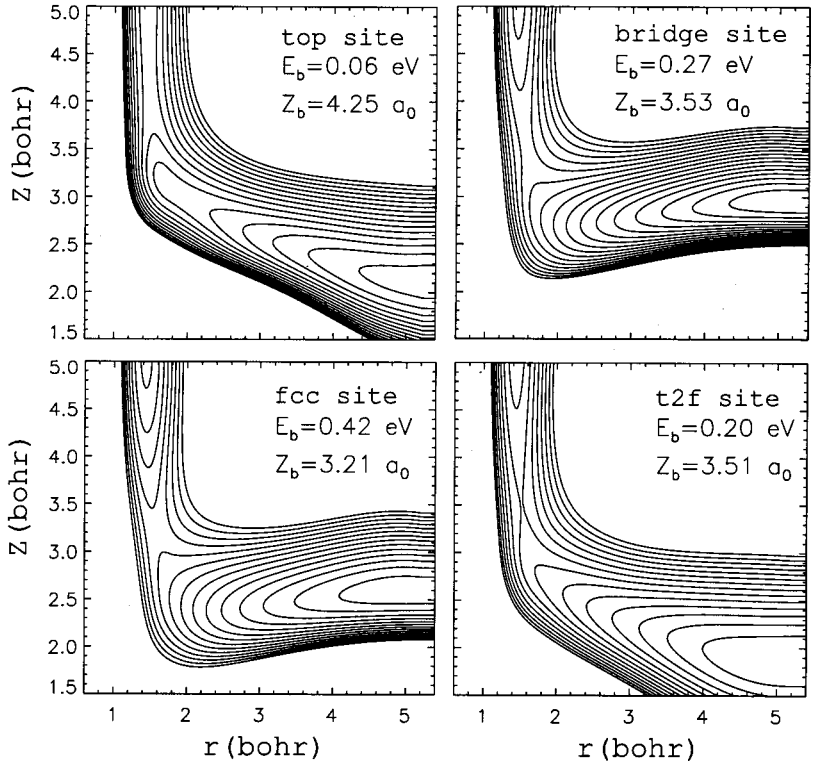

FIG. 3. 2D PES contour plots for four different impact sites on the Pt(111) surface. All plots correspond to H_2 being parallel to the surface, and $\phi=120°$. Indicated in each plot is the barrier height, E_b, and distance of the barrier to the surface, Z_b. The contour spacing is 0.1 eV and the potential is taken relative to the H_2 gas phase minimum.

region.[35] Even though this maximum error might seem large compared to the barrier height at some surface sites, in absolute sense it is quite small and the overall accuracy of the DFT-GGA PES is greater than has been achieved previously.

In Fig. 3 two-dimensional PESs calculated with DFT are shown for impact on four different surface sites. For each 2D PES, $\theta=90°$ (parallel orientation) and $\phi=120°$. The azimuthal angle ϕ is defined with respect to the *x*-axis (see Fig. 1). The top site corresponds to the coordinates $(x=0,y=0)$. The bridge site corresponds to coordinates $(x=L/2,y=L/2)$. The fcc site corresponds to $(x=L/3,y=L/3)$. The fourth site, the so-called t2f site, corresponds to $(x=L/6,y=L/6)$. The surface lattice constant $L=5.24$ bohr, and measures the distance between two neighboring Pt surface atoms.

All barriers are early and their height, E_b, varies from 0.06 eV (top site) to 0.42 eV (fcc site). There is also a substantial variation in the barrier distance to the surface, Z_b: from 3.21 to 4.25 bohr. This implies that the PES is both energetically and geometrically corrugated, where energetic corrugation refers to a variation of E_b across the surface, and geometric corrugation to a variation of Z_b across the surface.

C. Computational details

Table I lists the relevant parameters used in the 6D calculation for scattering of $(v=0,j=0)$ H_2 at normal incidence. To cover the collision energy range $E_i=0.05-0.55$ eV, two wave packet calculations were done for two separate energy ranges. This procedure is followed to avoid problems which could result from the interaction of low translational energy components in the wave packet with the optical potential if only one broad Gaussian initial wave packet would be used to cover $E_i=0.05-0.55$ eV for motion in *Z*.

Calculations were also done for $(v=1,j=0)$ and $(v=0,j=1,m_j=0,\pm1)$ H_2 at normal incidence, and for $(v=0,j=0)$ H_2 at off-normal incidence. In these calculations, the value of some parameters had to be adjusted relative to the $(v=0,j=0)$ calculations at normal incidence to obtain converged results.

In the $(v=0,j=0)$ H_2 calculation, 16 points in *x* and *y* had to be used for the low energy regime, and 20 points in *x* and *y* for the high energy regime. Also, for the high energy regime, a time step of 2.5 atomic units had to be used.

In the $(v=0,j=1,m_j=0,\pm1)$ H_2 calculations, the maximum *j* in the rotational basis used was 25, for both energy regimes.

In all off-normal incidence calculations the same value for the parameters were used. In both energy regimes, the numbers of points in *Z* used was 80 because a shorter optical potential could be used to obtain converged results. Also, the maximum *j* in the rotational basis used was 28. For the low energy regime, 20 points in *x* and *y* had to be used.

The projection operator formalism[36] was used to bring in the initial wave packet on a separate, long one-dimensional grid in order to be able to reduce the grid size in *Z* associated with the large scattering basis set.

To investigate reaction, calculations were performed for initial parallel translational energies, $E_\parallel$, of 0.0767, 0.230, and 0.690 eV. To investigate diffraction, additional calculations were performed for $E_\parallel=0.0555$ eV.

Probabilities $\geqslant 0.05$ are converged to within 1% of their absolute value. Probabilities between 0.01 and 0.05 are converged to within 3%. The absolute error in probabilities smaller than 1% is always smaller than 5×10^{-4}.

Downloaded 27 Mar 2011 to 130.37.129.78. Redistribution subject to AIP license or copyright; see http://jcp.aip.org/about/rights_and_permissions

TABLE I. List of input parameters and their values in the 6D calculation for dissociation of $v=0$ H_2 at normal incidence, for the energy ranges indicated. Values are in atomic units unless indicated otherwise.

Parameter	Energy range (eV) [0.05–0.16]	Energy range (eV) [0.15–0.55]
Initial wave packet		
Width ξ (bohr)	1.380	0.687
Initial position Z_0	11.0	10.0
Average initial momentum k_{z_0}	5.124	9.276
Grid parameters		
Z_i	−1.0	same
N_Z	90	80
N_Z^{sp}, # grid points specular grid	144	128
Grid spacing ΔZ	0.15	same
r_i	0.4	same
N_r	40	same
Grid spacing Δr	0.20	same
N_X	12	16
N_Y	12	16
Lattice constant L	5.23996	same
Maximum J in rotational basis	24	same
Time propagation		
Size time step Δt	2.5	5.0
Number of time steps	12 000	4 000
Optical potential in Z		
Initial value of range Z_{min}	7.1	same
Proportionality constant A_2	0.0018	0.0045
Range L_O	5.35	3.85
Optical potential in r		
Initial value of range r_{min}	4.20	same
Proportionality constant A_2	0.0096	same
Range L_O	4.0	same
Other parameters		
Analysis value Z_∞	7.1	same

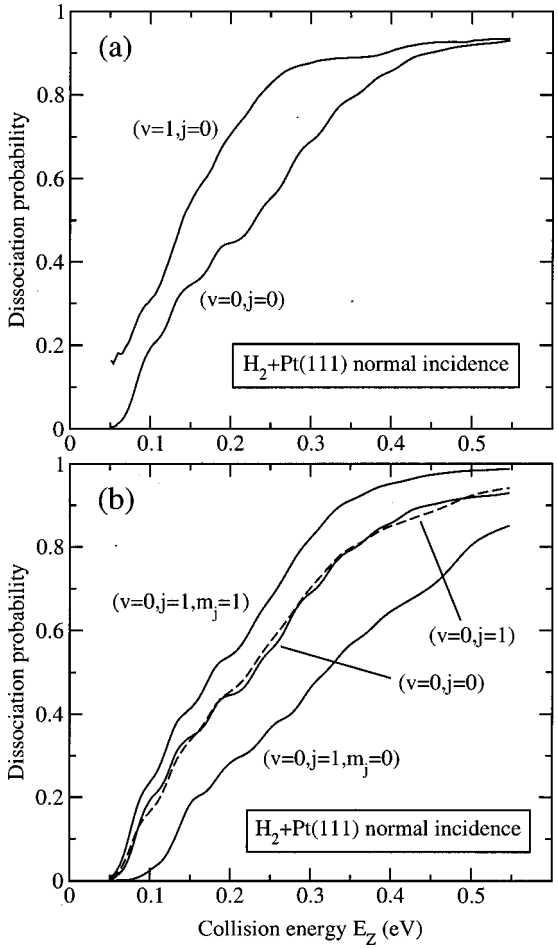

FIG. 4. Reaction probabilities from 6D calculations for normal incidence as a function of the collision energy E_Z. Results for initial $(v=0,j=0)$ and $(v=1,j=0)$ H_2 are shown in (a). Results for initial $(v=0,j=0)$, $(v=0,j=1,m_j=0)$, and $(v=0,j=1,m_j=1)$ H_2 are shown in (b). Also shown in (b) is the degeneracy averaged $(v=0,j=1)$ result (dashed line).

III. RESULTS AND DISCUSSION

A. Reaction for normal incidence

Reaction probabilities of initial $(v=0,j=0)$ and $(v=1,j=0)$ H_2, for normal incidence, are presented in Fig. 4(a), v and j being the vibrational and rotational quantum numbers, respectively. At the lowest collision energy for which results have been obtained ($E_Z=0.0513$ eV), the reaction probability of $(v=0,j=0)$ H_2 is 0.0051, and that of $(v=1,j=0)$ H_2 0.16. This means the ratio $P((v=1,j=0))/P((v=0,j=0))=32$, is much higher than was found in earlier 3D and 4D calculations[1,2] for this collision energy (see below), indicating that the vibrational enhancement is much larger in 6D than in 3D and 4D. Extrapolating both curves towards lower collision energies is expected to result in an even higher ratio.

In earlier 3D and 4D calculations on $H_2+Pt(111)$,[1,2] in which the molecule was always parallel to the surface, vibrational enhancement was also predicted, even though in those calculations the barrier to dissociation was always early. Halstead and Holloway[7] have investigated the effect of the barrier location on the reaction probability for initially vibrationally excited H_2 using a model PES. They found that for a late barrier, the vibrational energy that is released due to an increase of the reduced mass associated with the vibration perpendicular to the reaction path, will enhance the reaction probability. For an early barrier, however, the vibrational energy release, although present, occurs *after* the molecule has crossed the barrier (since there is almost no change of the reduced mass in the entrance channel), and therefore cannot be used to enhance the dissociation. In the 3D and 4D calculations, the vibrational enhancement of reaction was found to be due to a decreasing force constant in the entrance channel associated with the H_2 vibration, as the molecule approaches the barrier.[1,2] The same mechanism is also responsible for the vibrational enhancement of H_2 found in the present 6D calculations.

In Fig. 4(b), the reaction probability is shown for initial $(v=0,j=1,m_j=0)$ and $(v=0,j=1,m_j=1)$ H_2, for normal incidence, and compared with $(v=0,j=0)$ H_2. The reaction probability of the $(v=0,j=1,m_j=0)$ state is seen to be always smaller than that of the $(v=0,j=0)$ state. On the other hand, the reaction probability of the $(v=0,j=1,m_j=1)$ state is always larger than that of the $(v=0,j=0)$ state. These results are not unexpected, and can be understood by considering the preferred orientation of each rotational state, where ''preferred'' refers to the probability of finding the molecule with a particular orientation. For $(j=1,m_j=0)$ H_2, the preferred orientation will be in cones around the perpendicular orientation. For $(j=1,m_j=1)$ H_2, the preferred orientation

Downloaded 27 Mar 2011 to 130.37.129.78. Redistribution subject to AIP license or copyright; see http://jcp.aip.org/about/rights_and_permissions

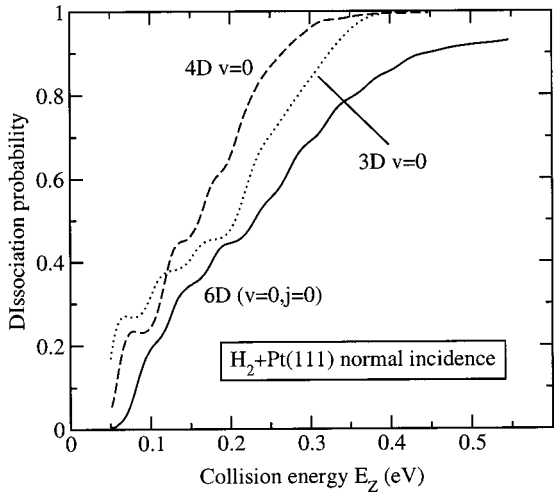

FIG. 5. Comparison of results of 3D, 4D, and 6D calculations for normal incidence as a function of the collision energy E_Z. The results are for $v=0$ H_2. In the 6D calculation $j=0$.

will be in cones around the parallel orientation, which is favourable for reaction. For $j=0$ H_2, all orientations are equally likely. Therefore, $(v=0,j=1,m_j=1)$ H_2 reacts better than $(v=0,j=0)$ H_2, which, in turn, reacts better than $(v=0,j=1,m_j=0)$ H_2. Similar results have been obtained in previous reduced dimensionality[37–45] and 6D calculations on H_2 dissociation on metals.[22,46–50] Also shown is the degeneracy averaged reaction probability curve of $(v=0,j=1)$ H_2, as would be obtained for a molecular beam in which all three m_j states for $j=1$ are equally populated. It deviates very little from the reaction probabilities for $(v=0,j=0)$ H_2.

In Fig. 5, results of 3D, 4D, and 6D calculations are compared for normal incidence. All results are for $v=0$ H_2, and $j=0$ in the 6D calculation. The origin of the difference between the 3D and 4D curves is discussed elsewhere.[2] The 6D probabilities are smaller than both the 3D and 4D probabilities for all collision energies. In the 3D and 4D calculations, the molecule was always oriented parallel to the surface, the most favourable orientation for dissociation. In the 6D calculation, rotation is also included, and for initial $j=0$, all orientations are equally probable. However, tilted orientations have large barriers to dissociation so that molecules in these orientations are less likely to react, and the presence of these unfavorable orientations reduce the reaction probability with respect to the 4D calculation. Previous 6D calculations on $H_2+Cu(100)$ likewise showed that inclusion of the rotational degrees of freedom leads to a decrease of the reaction probability.[51] For copper, the effect is larger due to barrier being later, leading to a stronger dependence of the potential barrier on the polar angle θ for Cu(100). The important effect of the rotation involving θ on the magnitude of the reaction probability was first pointed out in reduced dimensionality quantum dynamics calculations of Nielsen *et al.*[52]

The lowest barrier to dissociation, 0.06 eV, is for the parallel orientation above the top site, with dissociation towards the bridge site. However, in the 3D and 4D calculations, large probabilities were found for $E_Z<0.06$ eV. This was due to the same mechanism that caused reaction of $v=1$ H_2 to be vibrationally enhanced with respect to $v=0$, even though all barriers were early: a decrease of the force constant in the entrance channel[1] allows the release of vibrational energy to motion along the reaction coordinate. For initial $v=0$ H_2, zero-point vibrational energy was released in this way, resulting in significant reaction probabilities for $E_Z<0.06$ eV. In the 6D calculations, the reaction probability is <0.01 for $E_Z<0.06$ eV. This is in part due to the presence of unfavorable orientations, as explained above. However, it is also due to a quantum effect;[53,54] close to the surface, the rotational motion takes on the character of librational motion, and the quantization of this motion leads to a zero-point energy effect. For $j=0$, this results in an effective barrier to dissociation which is somewhat higher than the lowest barrier in the potential. In Table II, reaction probabilities of initial $v=0$ and $v=1$ H_2 are given for the 3D, 4D, and 6D calculations, at a collision energy of 0.0513 eV. Also given is their ratio $P(v=1)/P(v=0)$. For the 6D calculations this ratio is largest due to the small reaction probability of $v=0$ H_2 for $E_Z<0.06$ eV.

TABLE II. Reaction probabilities and ratios from 3D, 4D, and 6D calculations, for normal incidence and $E_Z=0.0513$ eV. Probabilities are given for initial $v=0$ and $v=1$ H_2. In the 3D and 4D calculations, the molecule is always parallel to the surface. The results of the 6D calculation are for $j=0$.

	3D	4D	6D
$P(v=0)$	0.187	0.0541	0.00514
$P(v=1)$	0.321	0.340	0.164
$P(v=1)/P(v=0)$	1.72	6.28	32.6

B. Reaction for off-normal incidence

In the wave packet calculations for off-normal incidence, the initial momentum parallel to the surface is fixed. Since the initial wave packet moving in Z contains a range of energies, the *actual* polar angle of incidence depends on E_Z according to

$$\theta_i=\tan^{-1}(\sqrt{(E_\parallel/E_Z)}), \tag{4}$$

where $E_\parallel$ is the parallel translational energy corresponding to the initial parallel momentum $K_\parallel$, and E_Z the collision energy corresponding to the momentum perpendicular to the surface, K_Z. In the 3D and 4D calculations,[1,2] an alternative "angle of incidence" was introduced to make a connection with experiment. This alternative angle, ϑ_i, is not a real angle but a measure of the amount of energy initially present in motion parallel to the surface. It is used for labelling purposes and easy reference in discussing the results. It is defined according to

$$\vartheta_i=\tan^{-1}(\sqrt{(E_\parallel/E_0)}). \tag{5}$$

In the above definition, E_0 is the dynamical barrier height of $(v=0,j=0)$ H_2 for normal incidence, which is defined as the collision energy E_Z for which the probability first becomes half its maximum value. From Fig. 4, the saturation values of the reaction probability for $(v=0,j=0)$ and

Downloaded 27 Mar 2011 to 130.37.129.78. Redistribution subject to AIP license or copyright; see http://jcp.aip.org/about/rights_and_permissions

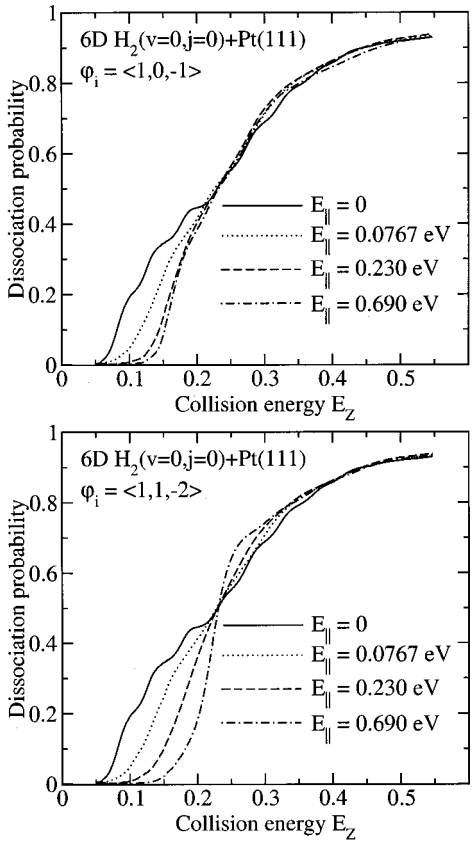

FIG. 6. Reaction probabilities of 6D calculations for off-normal incidence as a function of the normal collision energy E_Z. Results are for initial ($v=0,j=0$), for two different incidence directions. In the top panel, results are shown for incidence along the $\langle 10\bar{1}\rangle$ direction, and three different initial parallel energies, $E_\parallel$. In the bottom panel, results are given for incidence along the $\langle 11\bar{2}\rangle$ direction, for the same three initial parallel energies. The reaction probability for normal incidence is also indicated in each plot.

($v=1,j=0$) H_2 are estimated to lie between 0.90 and 0.95. However, for the purpose of defining ϑ_i through E_0, we assume here that the reaction probability saturates at 1, giving an E_0 of 0.23 eV for $v=0$. A special situation arises when $E_Z=E_0$. In this case, $\theta_i=\vartheta_i$, meaning that for this particular combination of E_Z and $E_\parallel$, the actual angle of incidence θ_i is given by ϑ_i.

Wave packet calculations have been done for two incidence directions: the $\langle 10\bar{1}\rangle$ and $\langle 11\bar{2}\rangle$ direction (see Fig. 2). For each incidence direction, calculations were done for $\vartheta_i=30°$, 45°, and 60°, corresponding to $E_\parallel=0.0767$ eV, 0.230 eV, and 0.690 eV, respectively. The results are presented in Fig. 6. The 6D results for reaction at off-normal incidence are in qualitative agreement with previous 4D results,[2] in that increasing the initial parallel energy inhibits reaction for low E_Z. Also, for incidence along the $\langle 10\bar{1}\rangle$ direction, increasing the initial parallel energy beyond 0.23 eV has (almost) no effect on the reaction for low E_Z, but does still have an effect on the reaction for incidence along the $\langle 11\bar{2}\rangle$ direction for low E_Z. This is true for both the 4D and 6D results.

There is only a quantitative difference between the 4D and 6D results for off-normal incidence, which is that, over the entire range of collision energies considered, the 6D reaction probability is reduced with respect to the 4D reaction probability. This was also noted in the results for normal incidence (see Fig. 4), where it was due to the presence of unfavorable orientations in the initial $j=0$ rotational state of H_2. This will also be true for off-normal incidence. Therefore, the 6D results can easily be understood in terms of the 4D results, keeping in mind that, for 6D, reaction will be hindered with respect to 4D due to the occurrence of unfavorable orientations. We will therefore be brief in explaining the 6D results for off-normal incidence, and refer to Ref. 2 for detailed explanations.

The effect of initial parallel momentum on the reaction has been investigated previously by Darling and Holloway,[55] who were the first to give an explanation for the low energy regime where reaction is hindered by parallel momentum. Gross[56] also investigated the high energy regime, which is of less interest for $H_2+Pt(111)$ because parallel momentum has a very small effect on the reaction of H_2 on Pt(111) in the high energy regime. In the low energy regime, reaction will dominated by parallel orientations or orientations very close to parallel. For parallel orientations, all barriers to dissociation are early, and ordered in such a way that the lowest barrier is located furthest from the surface and the barrier highest closest to the surface. As discussed in Ref. 55, a PES with such an ordering of barriers leads to a dependence of reaction on initial parallel momentum that is similar to that found for an energetically corrugated PES. Due to the parallel momentum, the incident molecule samples barriers across the whole unit cell. If it encounters a high barrier, it is likely to scatter back into the gas phase. Increasing the parallel momentum then obviously increases the probability that the incident molecule encounters a higher barrier, leading to decreased reaction. Therefore, for the PES discussed increased parallel momentum inhibits reaction in the low energy regime.

Increasing the initial parallel energy beyond 0.23 eV has a different effect on the reaction for both incidence directions considered. For incidence along the $\langle 10\bar{1}\rangle$ direction, increasing $E_\parallel$ has little or almost no effect on reaction, whereas for incidence along the $\langle 11\bar{2}\rangle$ direction, increasing $E_\parallel$ still has a large effect. This difference was also observed in previous 4D calculation,[2] and can be explained as follows: in the low energy regime, reaction is determined by the "reaction plane,"[2] which is the plane that contains the lowest barrier to dissociation, and is parallel to the incidence plane and perpendicular to the surface. For $H_2+Pt(111)$, the reaction plane must contain the top site, where the barrier is only 0.06 eV for the parallel orientation. At low E_Z, the reaction then takes place in the vicinity of the reaction plane.

In the reaction plane, the difference between the lowest and highest barrier for the parallel orientation determines when increasing the initial parallel energy (almost) stops having an effect on reaction. This difference will be called E_{corg}. Initial normal energy, E_Z, allows the molecule to climb up the barrier, whereas initial parallel energy, $E_\parallel$ sweeps the molecule across the surface. Once $E_\parallel > E_{\mathrm{corg}}$, motion parallel to the surface is undisturbed. In the $\langle 10\bar{1}\rangle$

Downloaded 27 Mar 2011 to 130.37.129.78. Redistribution subject to AIP license or copyright; see http://jcp.aip.org/about/rights_and_permissions

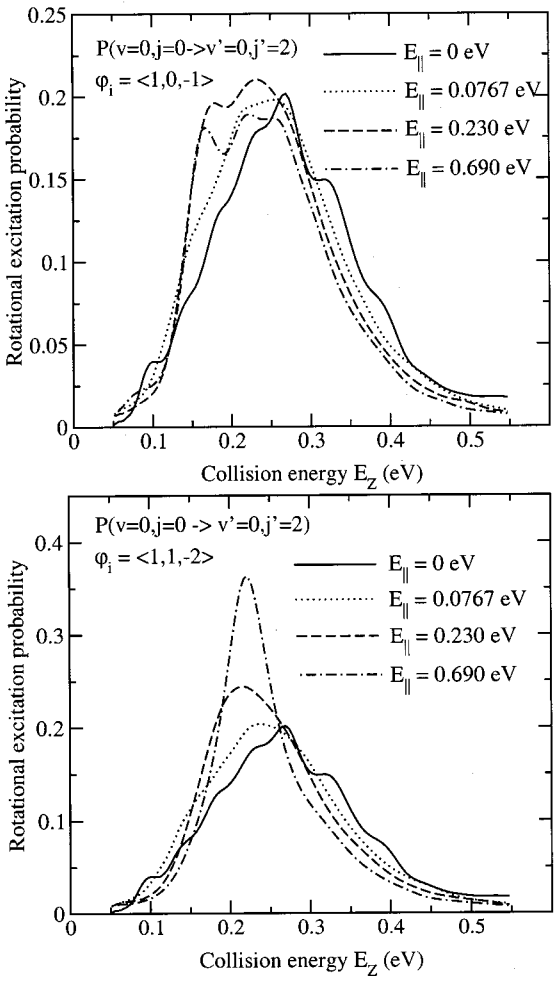

FIG. 7. Rotational excitation probabilities from 6D calculations for off-normal incidence, as a function of the collision energy E_Z. In the upper plot results are shown for incidence along the $\langle 10\bar{1}\rangle$ direction. In the lower plot results are shown for incidence along the $\langle 11\bar{2}\rangle$ direction. For both incidence directions, results have been calculated for the four values of the initial parallel energy $E_\parallel$ indicated.

reaction plane, $E_{\mathrm{corg}}=0.16$ eV, whereas in the $\langle 11\bar{2}\rangle$ reaction plane, $E_{\mathrm{corg}}=0.30$ eV.[2] Both values have been corrected for zero-point energy release.[1] This explains why in Fig. 6 for low E_Z, the reaction is no longer greatly effected for $E_\parallel>0.23$ eV for incidence along the $\langle 10\bar{1}\rangle$ direction. For incidence along the $\langle 11\bar{2}\rangle$ direction, $E_\parallel$ would be expected to cease having an effect for $E_\parallel>0.30$ eV, explaining that there is still a large difference between the curves for $E_\parallel=0.23$ and $E_\parallel=0.69$ eV.

In the high energy regime ($E_Z>0.23$ eV), the effect of $E_\parallel$ is to enhance the reaction for incidence along the $\langle 11\bar{2}\rangle$ direction, but only in a small energy interval. For even higher E_Z, reaction depends only on E_Z. For incidence along the $\langle 10\bar{1}\rangle$ direction, $E_\parallel$ has little effect on reaction, and depends almost entirely on E_Z. In summary, for collision energies $E_Z>0.40$ eV, reaction almost obeys normal energy scaling, independent of the incidence direction. In the 4D calculations,[2] the enhancement of the reaction for incidence along the $\langle 11\bar{2}\rangle$ direction was much stronger. Even for incidence along the $\langle 10\bar{1}\rangle$ direction, a clear, although small, enhancement was found for some E_Z. The enhancement of reaction for increasing $E_\parallel$ has been investigated previously by Gross.[56] Gross found that it occurs because the molecule has enough parallel momentum to climb up the maximum barrier where the propagation direction and potential gradient are almost aligned. Once at the top of the barrier, the molecule's propagation direction turns towards the surface and the molecule dissociates.[56] It is not completely understood why, for the high energy regime, the effect of initial parallel momentum is largest for incidence along the $\langle 11\bar{2}\rangle$ direction, and why the effect diminishes when including rotational motion (see also Ref. 2).

C. Rotational excitation

In Fig. 7 rotational excitation probabilities $P(v=0,j=0\rightarrow v'=0,j'=2)$ are presented for incidence along the $\langle 10\bar{1}\rangle$ and $\langle 11\bar{2}\rangle$ direction, for $\vartheta_i=0°$, 30°, 45°, and 60°. For incidence along the $\langle 10\bar{1}\rangle$ direction, the global trend is that excitation to $j=2$ is roughly independent of the initial parallel energy, i.e., rotational excitation roughly obeys normal energy scaling. For incidence along the $\langle 11\bar{2}\rangle$ direction, rotational excitation appears to be coupled to parallel motion more strongly; the probability curves get sharper with a higher maximum as the initial parallel energy increases. Also, the maximum in the rotational excitation probability tends to shift to lower energies, as the initial parallel momentum is increased. The curve for $E_\parallel=0.69$ eV peaks approximately at $E_Z=0.23$ eV.

Previous theoretical[57,58] and experimental[58,59] results show that large rotational excitation probabilities occur for collision energies E_Z close to the threshold energy to reaction, because the molecule is able to come close to the barrier where the potential contains a large amount of anisotropy. This explains why rotational excitation is found already for low E_Z; the lowest barrier in the PES to reaction is only 0.06 eV. Increasing E_Z will also increase the rotational excitation probability because a larger region (larger in X and Y) of the PES with high anisotropy becomes accessible to the molecule. The peaking behavior in Fig. 7 (i.e., the fact that the rise in the rotational excitation probabilities is followed by a decrease) could be caused by two competing channels: a strong competition with excitations to $j'=4$ for $E_Z>0.25$ eV, or competition with reaction. Although an increase in the probability of excitation to $j'=4$ is found, it is too small to account for the decrease in the probability for excitation to $j'=2$. This suggests that the decrease found is due to an increase of the reaction probability, and indicates a correlation between the two.

Support for the existence of a correlation between rotational excitation and reaction comes from hindering of rotational excitation by parallel motion for low E_Z, in the same manner as was found for reaction for off-normal incidence. Especially for incidence along the $\langle 11\bar{2}\rangle$ direction, initial parallel momentum inhibits rotational excitation, albeit over a much smaller energy interval (i.e., 0.075–0.15 eV) than for reaction (compare Figs. 6 and 7). In this small interval, the ordering of the curves almost follows that of reaction for off-normal incidence.

Downloaded 27 Mar 2011 to 130.37.129.78. Redistribution subject to AIP license or copyright; see http://jcp.aip.org/about/rights_and_permissions

TABLE III. Shown is the anisotropy in θ and ϕ of the potential at the reaction barrier geometry for the four impact sites shown in Fig. 3. Also given is the barrier location, (Z_b, r_b), and barrier height, E_b, of each impact site. The anisotropy in θ is the difference between the smallest value of V and the largest value of V, for the four sites and values of Z_b and r_b indicated in the table, and $\phi = 120°$. The anisotropy in ϕ is the difference between the maximum and minimum value of V for $\theta = 90°$.

	Barrier			Anisotropy (eV)	
Site	Z_b (bohr)	r_b (bohr)	E_b (eV)	θ	ϕ
top	4.25	1.46	0.06	0.15	0.001
t2f	3.51	1.52	0.20	0.40	0.020
fcc	3.21	1.58	0.42	0.27	0.004
bridge	3.53	1.55	0.27	0.23	0.099

To understand why rotation is more strongly coupled to parallel motion for incidence along the $\langle 11\bar{2} \rangle$ direction than for incidence along the $\langle 10\bar{1} \rangle$ direction, we consider the anisotropy at the barrier as a function of the barrier position within the unit cell. For rotational excitations to occur at all, the potential must be anisotropic in the region in front of the barrier (once the molecule has crossed the barrier there is little chance it will go back). For rotational excitations to depend on the initial parallel momentum, a coupling must exists between rotation and parallel translation.

In Table III the anisotropy in θ and ϕ at the barrier position is given for the four sites of Fig. 3. For all sites, the ϕ anisotropy is very small and will be of minor importance. The θ anisotropy, however, varies quite a lot, from 0.15 eV for the top site to 0.40 eV for the t2f site, with the other two sites lying in between.

For an understanding of the qualitative behavior of the results in Fig. 7, it suffices to consider the reaction plane (see Sec. III B). For incidence along the $\langle 10\bar{1} \rangle$ direction, the reaction plane contains the top site and the bridge site. As Table III shows, the difference in anisotropy between these two sites is only 0.08 eV (0.15 eV vs 0.23 eV). This indicates a weak coupling between rotation and translation along the $\langle 10\bar{1} \rangle$ direction. For incidence along the $\langle 11\bar{2} \rangle$ direction, the reaction plane contains both the top site and t2f site. According to Table IV, the difference in anisotropy is 0.25 eV, much larger than for incidence along the $\langle 10\bar{1} \rangle$ direction, indicating a larger coupling between rotation and translation for incidence along the $\langle 11\bar{2} \rangle$ direction. This explains why the rotational excitation probability shows a much larger dependence on initial parallel energy for the $\langle 11\bar{2} \rangle$ direction, as observed in our results.

TABLE IV. Compared are the ratios of zero **G** to nonzero **G** diffraction probability for in-plane scattering. Values are given for the experiment of Cowin *et al.* (Ref. 5), and for the present 6D and previous 4D calculations (Ref. 2). The translational energies are $E_\parallel = 0.0555$ eV and $E_Z = 0.0555$ eV.

	$\langle 10\bar{1} \rangle$, in-plane $P(\mathbf{G}=0)/P(\mathbf{G}\neq 0)$	$\langle 11\bar{2} \rangle$, in-plane $P(\mathbf{G}=0)/P(\mathbf{G}\neq 0)$
Cowin *et al.*	100	10
Theory (4D)	16.5	4.21
Theory (6D)	20.0	4.71

The peaking behavior found for incidence along the $\langle 11\bar{2} \rangle$ direction occurs in the regime where reaction is hindered by parallel motion, but where the molecule *is* able to come close to the barriers where it can be rotationally excited. Because the coupling between parallel translational and rotational motion is strongest along the $\langle 11\bar{2} \rangle$ direction, allowing efficient energy transfer from parallel translational motion to rotational motion (see above), it is expected that for incidence along the $\langle 11\bar{2} \rangle$ direction, the curve will rise to a higher maximum for higher initial parallel momentum, as shown by our results (see Fig. 7). The decrease of $P(v=0, j=0 \rightarrow v'=0, j'=2)$ for higher E_Z is due to reaction becoming more and more important, until eventually about 95% of all molecules react.

D. Diffraction

Previous 4D calculations[2] showed that, for $E_\parallel = 0.48$ eV, out-of-plane diffraction occurred with large probabilities for incidence along the $\langle 10\bar{1} \rangle$ direction [see Fig. 6(b) of Ref. 2]. However, for incidence along the $\langle 11\bar{2} \rangle$ direction, out-of-plane diffraction was out-competed by specular reflection. In Fig. 8 probabilities of scattering into the zeroth and first diffraction order (P_0 and P_1) are plotted, for incidence along the $\langle 10\bar{1} \rangle$ and $\langle 11\bar{2} \rangle$ direction, and for $E_\parallel = 0.69$ eV. Note that these are the total diffraction probabilities, including rotationally elastic and inelastic diffraction. The results are consistent with previous 4D calculations;[2] for incidence, along the $\langle 10\bar{1} \rangle$ direction, the probability of diffraction into the first diffraction order (sum of six diffraction channels) is larger than the probability of specular scattering for $E_Z > 0.1$ eV. The difference is largest for $E_Z \approx 0.14$ eV. For incidence along the $\langle 11\bar{2} \rangle$ direction, specular scattering is more likely than first order diffraction over the entire energy regime considered. The difference gets smaller for larger E_Z.

By also plotting in Fig. 8(a) the probability of *rotationally elastic* diffraction into the zeroth and first diffraction order, P_0^{el} and P_1^{el}, respectively, it is demonstrated that, for $E_Z < 0.2$ eV, the larger part of first order diffraction is rotationally elastic for low E_Z. Also plotted in Fig. 8(a), for a number of collision energies, is the summed probability of *rotationally elastic* diffraction into the (0,1) and (0,−1) diffraction states, $\overline{P}_1^{\mathrm{el}}$. Comparing P_1^{el} and $\overline{P}_1^{\mathrm{el}}$ shows that almost all probability of rotationally elastic diffraction goes into these two channels. For incidence along the $\langle 11\bar{2} \rangle$ direction [Fig. 8(b)], most of the rotationally elastic first order diffraction likewise occurs into two diffraction states, i.e., the out-of-plane (0,−1) and (−1,0) diffraction states.

These results are consistent with the 4D calculations[2] and can, therefore, be understood within the 4D model. We will briefly discuss these results and refer to Ref. 2 for a more detailed discussion.

We will first discuss the results for incidence along the $\langle 10\bar{1} \rangle$ direction. The fact that, for large initial parallel energy, the computed first order rotationally elastic diffraction

Downloaded 27 Mar 2011 to 130.37.129.78. Redistribution subject to AIP license or copyright; see http://jcp.aip.org/about/rights_and_permissions

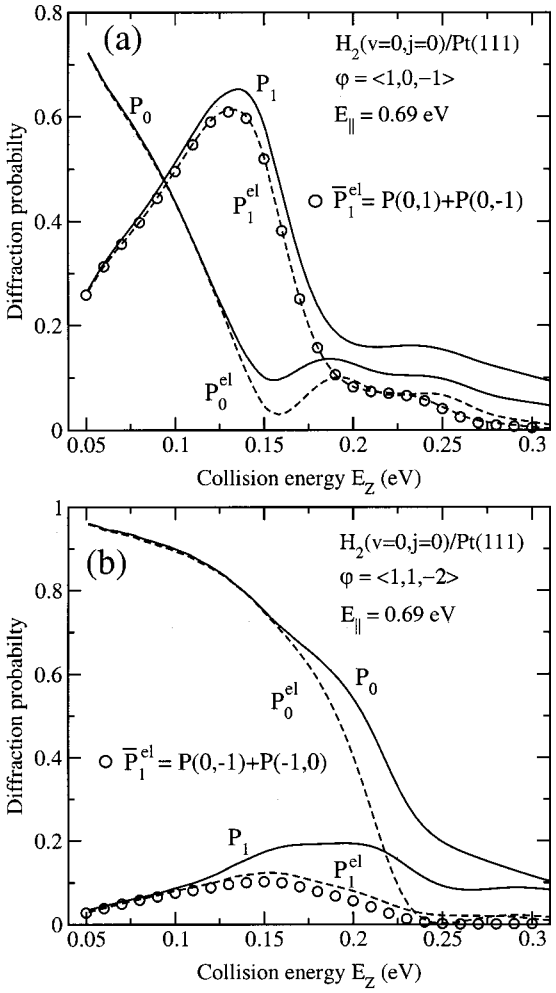

FIG. 8. Shown are the total probabilities of diffraction into the zeroth and first diffraction order, P_0 and P_1, respectively, for incidence along the $\langle 10\bar{1}\rangle$ (a) and $\langle 11\bar{2}\rangle$ (b) direction. Also shown for both incidence directions is the rotationally elastic diffraction probability into the zeroth and first diffraction order, P_0^{el} and P_1^{el}, respectively. Shown in (a) is the part of P_1^{el} due to diffraction into the (0,1) and (0,−1) out-of-plane diffraction states, $\bar{P}_1^{\mathrm{el}}$. Shown in (b) is the part of P_1^{el} due to diffraction into the (0,−1) and (−1,0) out-of-plane diffraction states, $\bar{P}_1^{\mathrm{el}}$.

occurs almost entirely into the (0,1) and (0,−1) diffraction states is due to two factors. The first is that the potential shows the largest corrugation along the $\langle 11\bar{2}\rangle$ crystal direction (see Fig. 7 of Ref. 2). All first order diffraction states correspond to a momentum change in this highly corrugated direction. On the basis of this argument alone one would expect to find large diffraction probabilities for *all* six first order diffraction states. However, the energy transfer associated with diffraction into the (0,1) and (0,−1) states is independent of the initial momentum because the momentum change associated with these two states is perpendicular to the plane of incidence. For the other four first order diffraction states, there is a component that is parallel to the plane of incidence, and therefore scattering into these states requires a larger energy transfer, which leads to decreased probabilities for transitions into these states.[2]

For incidence along the $\langle 11\bar{2}\rangle$ direction specular scattering dominates over first order diffraction over the entire energy regime considered. Plotted in Fig. 8(b) are the diffraction probabilities P_0 and P_1, the rotationally elastic diffraction probabilities P_0^{el}, P_1^{el} and the summed probability of rotationally elastic diffraction into the (0,−1) and (−1,0) states, $\bar{P}_1^{\mathrm{el}}$. First order diffraction is much smaller than specular scattering for $E_Z < 0.2$ eV. Because all first order diffraction states correspond to a momentum change in the $\langle 11\bar{2}\rangle$ crystal direction, which is highly corrugated, one would expect to find large diffraction probabilities into all first order states. However, as mentioned above, if the energy transferred is large with respect to the available energy in motion normal to the surface, the diffraction will be less efficient. This is why, for low E_Z, only the (0,−1) and (−1,0) diffraction states occur with largest probability, because these states have the smallest energy gap with respect to the (0,0) diffraction state. Furthermore, for these two diffraction states the energy transfer is in a favorable direction, i.e., energy is transferred from motion parallel to the surface, in which a lot of energy is available, to motion normal to the surface, in which less energy is available.[2]

E. Comparison with experiment: Reaction

The present 6D calculations allow for a full comparison with experiment. Molecular beam results on reaction of D_2 on Pt(111) are available from different groups.[4,60] Here, we will compare our results with experimental results of Luntz *et al.*[4] for reasons discussed in Ref. 61. Although the results are for D_2 on Pt(111), Luntz *et al.* could not detect any measurable difference between H_2 and D_2 reacting on Pt(111) at normal incidence, validating a comparison with our theoretical results for H_2 if the assumption is made that an isotope effect is also absent for off-normal incidence.

In Fig. 9(b) experimental reaction probabilities measured by Luntz *et al.*[4] are compared with theoretical reaction probabilities. The overall agreement with experiment is quite good. For the values of ϑ_i considered, theory predicts reaction probabilities that are too small just above the onset energy, and too high for higher E_i relative to the onset energy. A reaction probability that is too small just above the onset energy suggests that the lowest barrier is somewhat too high. Further discrepancies may be explained in several ways. First of all, inaccuracies in the DFT-GGA PES, i.e., too little anisotropy and/or corrugation of the reaction barrier height could lead to a width of the reaction curve that is too small. Second, the calculations are for a 0 K surface. Including the effect of surface temperature may lead too larger reaction probabilities for low E_i and smaller reaction probabilities for higher E_i (which is precisely what is needed), as found in experiments on $H_2+Cu(111)$.[62] However, Luntz *et al.*[4] found the effect of surface temperature on reaction to be quite small, even at a E_i as low as 75 meV.[4] The discrepancies can also be due to the wide rotational state distribution in the incident molecular beam in the experiment. For many H_2+metal surface systems, the reaction probability depends on the initial angular momentum of the incident molecule, which will broaden the reaction probability curve in an molecular beam experiment relative to the computational results for $j=0$.[41,43,50,63–65] Presently, we have results for too few

Downloaded 27 Mar 2011 to 130.37.129.78. Redistribution subject to AIP license or copyright; see http://jcp.aip.org/about/rights_and_permissions

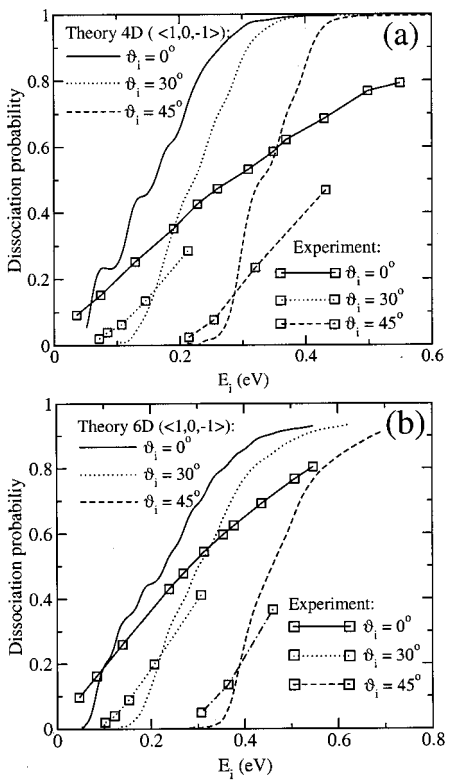

FIG. 9. Reaction probabilities from 4D (a) and 6D (b) calculations of $H_2+Pt(111)$ are compared with experimental values of Luntz *et al.* (Ref. 4) for $D_2+Pt(111)$. The angle ϑ_i is related to the initial parallel momentum through Eq. (5), where $E_0=0.16$ eV and 0.23 eV, for 4D and 6D, respectively.

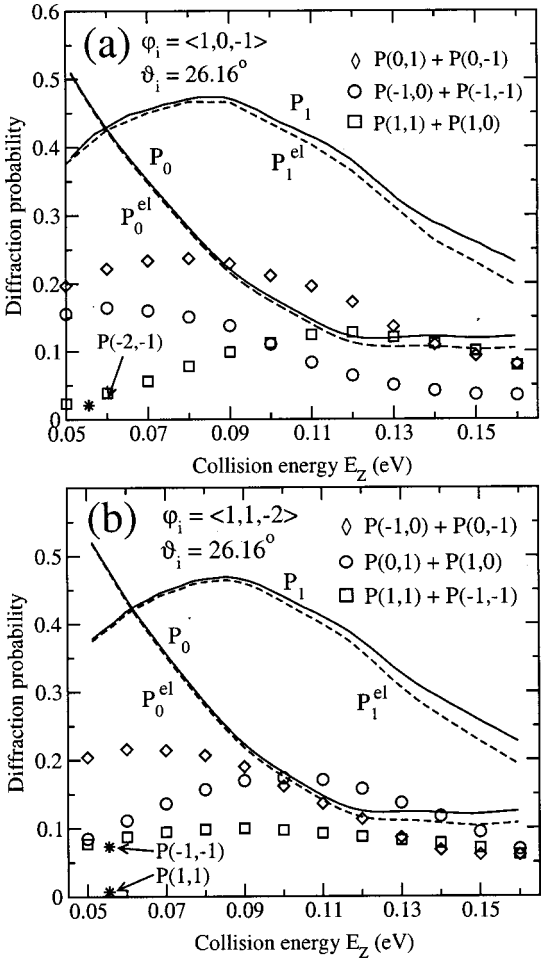

FIG. 10. Total diffraction probabilities for diffraction into the zeroth and first diffraction order, P_0 and P_1, respectively, are shown as a function of the collision energy normal to the surface, E_Z, for incidence along the $\langle 10\bar{1}\rangle$ (a) and $\langle 11\bar{2}\rangle$ (b) direction. The initial parallel energy $E_\parallel=0.0555$ eV. Also shown for both incidence directions is the rotationally elastic diffraction into the zeroth and first diffraction order, P_0^{el} and P_1^{el}, respectively. Then, P_1^{el} is decomposed into pairs of diffraction states (see Sec. III F). The asterisks indicate the rotationally elastic diffraction probability into the lowest order in-plane diffraction states for each incidence direction, for $E_Z=0.0555$ eV. For these values of E_Z and $E_\parallel$, the experimental conditions of Cowin *et al.* (Ref. 5) for an incidence angle $\theta_i=45°$ are exactly reproduced.

j-states to estimate the importance of this effect.

The effect of including additional degrees of freedom, while comparing the results with experiment, in going from a 4D to a 6D model is demonstrated by Figs. 9(a) and 9(b). Clearly, by including the rotational degrees of freedom, the agreement with experiment gets better, as expected. The effect of including rotation has been explained before; due to the presence of unfavorable orientations of the incident molecule, the reaction probability is reduced with respect to the case in which a molecule is always parallel to the surface, as in the 4D model. Note that we find that the agreement between theory and experiment improves not only for normal incidence but also for off-normal incidence, suggesting that the DFT-GGA PES used describes the reaction of H_2 on Pt(111) quite well.

F. Comparison with experiment: Diffraction

An intriguing question concerning the $H_2+Pt(111)$ system is why the molecular beam experiment of Luntz *et al.*[4] on the reaction of D_2 on Pt(111) suggests the PES to be corrugated (reaction not obeying normal energy scaling), whereas molecular beam experiments of Cowin *et al.*[5] on rotationally (in)elastic scattering of HD from Pt(111) suggest the PES to be flat (very little in-plane diffraction was found, but no effort was made to observe out-of-plane diffraction). However, as demonstrated in Sec. III D, for $\vartheta_i>45°$, almost all first order diffraction is out-of-plane, and only very little in-plane, suggesting that proof of a corrugated $H_2+Pt(111)$ PES is to be found in measurements of out-of-plane scattering for $\vartheta_i>45°$. The question is then if this prediction also holds for smaller ϑ_i, which would then explain why so little diffraction was found in the experiments of Cowin *et al.*[5]

In Figs. 10(a) and 10(b) theoretical calculations of diffraction probabilities are presented for $\vartheta_i=26.16°$. For this value of ϑ_i, and $E_Z=0.0555$ eV, $\theta_i=45°$, which corresponds to the experimental conditions in one of the experiments of Cowin *et al.*[5] for which they provided exact numbers of ratios (zero **G** diffraction/nonzero **G** in-plane diffraction), where **G** is a surface reciprocal lattice vector which corresponds to a particular diffraction state, for both the $\langle 10\bar{1}\rangle$ and $\langle 11\bar{2}\rangle$ incidence incidence directions. Therefore, a direct comparison can be made.

In Fig. 10 several probabilities are shown. The probabili-

Downloaded 27 Mar 2011 to 130.37.129.78. Redistribution subject to AIP license or copyright; see http://jcp.aip.org/about/rights_and_permissions

ties P_0 and P_1 correspond to the total diffraction probability into the zeroth and first order diffraction states, respectively. The probabilities P_0^{el} and P_1^{el} correspond to rotationally elastic scattering into the zeroth and first order diffraction states. The first diffraction order consists of six diffraction states. For the $\langle 10\bar{1}\rangle$ direction, three pairs of diffraction states can be identified such that, due to symmetry, for each pair the diffraction probability is the same for both states making up the pair. For the $\langle 11\bar{2}\rangle$ direction, two such pairs can be identified, and another pair can be formed by combining the forward and backward diffraction states, (1,1) and $(-1,-1)$. The probability P_1^{el} is then decomposed into these three diffraction pairs. This provides a clear view of which channels carry most of the diffraction probability. What is immediately obvious is that, in contrast with the results for $\vartheta_i > 45°$ in Fig. 8, the diffraction probability is not exclusively (or almost exclusively) going into one pair of diffraction states. This is true for both incidence directions. In fact, the total probability is distributed over the three diffraction pairs, not necessarily preferring one over the other at high E_i. The total first order diffraction probability, P_1^{el}, is rather substantial compared to the specular scattering probability, P_0^{el}. For $E_Z > 0.06$ eV, P_1^{el} is larger than P_0^{el}, with a maximum difference between the two occurring for $E_Z \approx 0.11$ eV.

As mentioned, Cowin *et al.* measured the ratio (zero **G** diffraction/nonzero **G** in-plane diffraction), where in both cases the diffraction includes rotationally elastic and rotationally inelastic scattering. For incidence along the $\langle 10\bar{1}\rangle$ direction, the lowest order in-plane diffraction state is the $(-2,-1)$ state. This state corresponds to backward scattering, i.e., the molecule loses momentum parallel to the surface. The lowest order in-plane diffraction state that corresponds to forward scattering, the (2,1) diffraction state, is closed at the experimental incidence energy. Indicated in Fig. 10(a) is the rotationally elastic diffraction probability for scattering into the $(-2,-1)$ diffraction state at $E_Z = 0.0555$ eV, matching the conditions of Cowin *et al.* At this energy, the $(-2,-1)$ channel makes up 89% of the total (rotationally elastic and inelastic) in-plane diffraction probability. For incidence along the $\langle 11\bar{2}\rangle$ direction, the lowest order in-plane diffraction states are the (1,1) and $(-1,-1)$ states, belonging to the first diffraction order and corresponding to forward and backward diffraction, respectively. They are both open channels for $E_Z = E_{\parallel} = 0.0555$ eV. Indicated in Fig. 10(b) are the theoretical probabilities of rotationally elastic diffraction into these two states. Together they make up 79% of the total in-plane diffraction probability. Another 15% goes into the $(-2,-2)$ in-plane rotationally elastic diffraction state.

In Table IV, the experimental ratios of Cowin *et al.*[5] are compared with the theoretical ratios from 4D and 6D calculations. There are still substantial discrepancies between experiment and theory. However, there is a slight improvement in going from 4D to 6D. Possible reasons for the deviations between experiment and theory will be discussed below. First we will discuss the paradox presented by the experiments of Luntz *et al.*[4] and Cowin *et al.*[5] As discussed above, in the molecular beam experiment of Luntz *et al.* on sticking of D_2 on Pt(111), they found that the sticking probability does *not* scale with the translational energy in motion normal to the surface, i.e., normal energy scaling was not obeyed. This suggests that the potential must be corrugated. On the other hand, molecular beam experiments of Cowin *et al.* on rotationally inelastic scattering of HD from Pt(111) showed that there was very little diffraction, suggesting a flat potential. The present 6D calculations on reaction and diffraction of H_2 from Pt(111) shed some light on this paradox.

An important piece of the puzzle is to be found in diffraction. In the experiment by Cowin *et al.*,[5] only *in-plane* diffraction was measured. As demonstrated in Fig. 10, in-plane diffraction constitutes only a small contribution to the computed total diffraction probability. For incidence along the $\langle 10\bar{1}\rangle$ direction, the computed total in-plane diffraction probability is only 0.023 at the energies used by Cowin *et al.* However, there is a lot of diffraction into the first diffraction order [see Fig. 10(a)], which consists of six diffraction states. At the experimental conditions of Cowin *et al.*, the total probability of first order diffraction is 0.40, compared to a total probability of zero **G** scattering of 0.47. However, all first order diffraction states are *out-of-plane* and therefore not measured in the experiment.

For incidence along the $\langle 11\bar{2}\rangle$ direction, the story is much the same. The total probability of in-plane diffraction is 0.10. The lowest order in-plane diffraction channels belong to the first diffraction order. Together they take only 0.080 diffraction probability of a total first order diffraction probability of 0.39, compared to a total probability of zero **G** scattering of 0.48. The two in-plane first order diffraction channels only take little of the total first order diffraction probability. The other four first order diffraction states are out-of-plane and therefore not measured in experiment.

In conclusion, theory predicts substantial diffraction, which is proof of a corrugated surface potential. In the experiment of Cowin *et al.*, only little diffraction was found because only in-plane diffraction was measured. However, we predict that out-of-plane diffraction is much more important, for both incidence directions. So, any scattering experiment that wishes to address the amount of corrugation of the H_2+Pt(111) system, should also look at out-of-plane diffraction.

Finally, we wish to comment on the fact that Cowin *et al.* used HD instead of H_2. Because the center-of-mass of HD does not coincide with its geometrical center-of-mass, the potential will be strongly anisotropic. This could well result in a strong competition between rotational excitation and diffraction. This could explain why the experimental ratios of zero **G** scattering to nonzero **G** in-plane diffraction measured for HD are larger than our theoretical ratios computed for H_2. We hope to address this issue in future research.

IV. CONCLUSION

We have used a time-dependent wave packet (TDWP) method to study reactive and rotationally (in)elastic diffractive scattering of H_2 from Pt(111). In the model used all six molecular degrees of freedom of H_2 are treated quantum

Downloaded 27 Mar 2011 to 130.37.129.78. Redistribution subject to AIP license or copyright; see http://jcp.aip.org/about/rights_and_permissions

mechanically. The present six-dimensional (6D) calculations follow earlier 3D (Ref. 1) and 4D (Ref. 2) calculations. The main motivation for studying $H_2+Pt(111)$ is the contradicting conclusions from two molecular beam experiments; in the experiment of Luntz *et al.*[4] on sticking of D_2 on Pt(111), it was concluded that the potential energy surface (PES) must be corrugated since sticking did not obey normal energy scaling. However, in the experiment of Cowin *et al.*[5] on rotationally (in)elastic diffraction of HD from Pt(111) very litte diffraction was found, suggesting a flat surface.

The PES was constructed by interpolating 14 2D PESs for four different sites and various orientations with respect to the surface.[35] A corrugation reducing procedure[11] was used to interpolate the 2D PES to form a 6D PES.

Reaction of $(v=1,j=0)$ H_2 is enhanced with respect to $(v=0,j=0)$ H_2. A similar enhancement was also found in the 3D (Ref. 1) and 4D (Ref. 2) calculations. It is not due to a reduced mass effect[7] because the barriers where reaction will predominantly occur (barriers for the parallel orientation) are all located in the entrance channel. Instead vibrational enhancement is due to a decrease of the force constant associated with the molecular vibration, as the molecule approaches the barrier.

Calculations for initial $(v=0,j=1,m_j=0,\pm 1)$ show that reaction of $(v=0,j=1,m_j=0)$ is decreased with respect to $(v=0,j=1,m_j=\pm 1)$. This is due to $(v=0,j=1,m_j=0)$ resembling more of a cartwheel-like rotation and $(v=0,j=1,m_j=\pm 1)$ resembling more of a helicopter-like rotation.

The 6D reaction probabilities for normal incidence with $j=0$ were smaller than in 4D. This is due to the presence of unfavorable orientations in the 6D model. In the 4D model, the molecule was always oriented parallel to the surface, which is the most favorable orientation for reaction. In the 6D model, the molecule's orientation is determined by its initial rotational state, and initial molecular orientations that are tilted with respect to the parallel orientation are present. Because the barrier to dissociation is larger for tilted orientations than for parallel orientations, a smaller reaction probability is found in the 6D model than in the 4D model.

The present 6D calculations for reaction of H_2 on Pt(111) at normal and off-normal incidence are in good agreement with the results of molecular beam experiments of Luntz *et al.*[4] on the sticking of D_2 on Pt(111). The agreement is improved for both normal and off-normal incidence in going from 4D to 6D by adding the rotational degrees of freedom. Also, the general trend found for reaction at off-normal incidence in the 3D, 4D, and 6D calculations is the same; parallel momentum inhibits reaction for low collision energies E_Z. The explanation for this effect was given first by Darling and Holloway;[55] because the molecule's parallel momentum tends to sweep the molecule across the unit cell, it is more likely to encounter a high barrier from which it can scatter back into the gas phase. Obviously, for higher parallel momentum, the chance of encountering a high barrier is larger, explaining why increasing the initial parallel momentum of the molecule decreases its reaction probability at low incidence energies.

For higher collision energies, parallel momentum leads to a small enhancement of reaction for incidence along the $\langle 11\bar{2}\rangle$ direction, and has almost no effect for incidence along the $\langle 10\bar{1}\rangle$ direction. For incidence along the $\langle 11\bar{2}\rangle$ direction, parallel momentum leads to the largest enhancement in the 3D calculations.[1] In the 4D calculations, the enhancement is already substantially smaller,[2] and it is smallest in the 6D calculations.

Finally, a comparison was made with molecular beam experiments of Cowin *et al.*[5] on rotationally inelastic diffraction of HD from Pt(111). They found very little diffraction. This is in contrast with sticking measurements of Luntz *et al.*[4] who concluded that the potential must be rather corrugated. On this basis one would expect substantial diffraction. However, Cowin *et al. only* looked at in-plane diffraction. In previous 4D calculations,[2] it was shown that for larger angles of incidence, competition with out-of-plane diffraction leads to a strong decrease of in-plane diffraction. This result has been confirmed in our 6D calculations, for initial parallel momentum $E_{\parallel}>0.23$ eV. To make a more direct comparison with the experiment of Cowin *et al.*, we also did a calculation that reproduced the exact conditions of the experiment of Cowin *et al.*, i.e., an incidence angle $\theta_i=45°$ and $E_Z=55.5$ meV. For both the $\langle 10\bar{1}\rangle$ and $\langle 11\bar{2}\rangle$ incidence direction we found that the total first order diffraction probability, which consists of six diffraction states, was comparable to the specular reflection probability. For incidence along the $\langle 10\bar{1}\rangle$ direction, the lowest order in-plane diffraction state is of second order, implying that *no* first order diffraction is measured at all. For incidence along the $\langle 11\bar{2}\rangle$ incidence direction, there are two in-plane diffraction states of the first order. However, they take only a small fraction of the total first order diffraction probability.

The main conclusion with respect to the paradox presented by the molecular beam experiments of Luntz *et al.*[4] and Cowin *et al.*[5] is that the measurements do not represent a true contradiction. The diffraction experiment obtained insufficient data for our purpose; only in-plane diffraction was considered, while out-of-plane diffraction, where evidence of the corrugation will be most manifest, was ignored.

ACKNOWLEDGMENTS

E.P. and G.J.K. gratefully acknowledge the Stichting Nationale Computerfaciliteit (NCF) for generous grants of computation time. R.A.O. and E.J.B. are grateful for funding by the National Research School Combination ''Catalysis by Design.'' We are grateful to D. Lemoine and M.F. Somers for implementing the FBR-DVR scheme for rotational motion in our scattering code. Also, we would like to thank H.F. Busnengo and A. Salin for their help in providing an accurate representation of the $H_2+Pt(111)$ potential. Finally, we are grateful to A. C. Luntz and A. Hodgson for useful discussions.

[1] E. Pijper, G. J. Kroes, R. A. Olsen, and E. J. Baerends, J. Chem. Phys. **113**, 8300 (2000).
[2] E. Pijper, G. J. Kroes, R. A. Olsen, and E. J. Baerends, J. Chem. Phys. **116**, 9435 (2002).
[3] G. R. Darling and S. Holloway, Surf. Sci. **304**, L461 (1994).
[4] A. C. Luntz, J. K. Brown, and M. D. Williams, J. Chem. Phys. **93**, 5240 (1990).

Downloaded 27 Mar 2011 to 130.37.129.78. Redistribution subject to AIP license or copyright; see http://jcp.aip.org/about/rights_and_permissions

[5] J. P. Cowin, C. F. Yu, S. J. Sibener, and L. Wharton, J. Chem. Phys. **79**, 3537 (1983).
[6] G. R. Darling and S. Holloway, Rep. Prog. Phys. **58**, 1595 (1995).
[7] D. Halstead and S. Holloway, J. Chem. Phys. **93**, 2859 (1990).
[8] A. Gross and M. Scheffler, Chem. Phys. Lett. **256**, 417 (1996).
[9] D. Wetzig, M. Rutkowski, H. Zacharias, and A. Gross, Phys. Rev. B **63**, 205412 (2001).
[10] R. Kosloff, J. Phys. Chem. **92**, 2087 (1988).
[11] H. F. Busnengo, A. Salin, and W. Dong, J. Chem. Phys. **112**, 7641 (2000).
[12] A. D. Becke, Phys. Rev. A **38**, 3098 (1988).
[13] J. P. Perdew, Phys. Rev. B **33**, 8822 (1986).
[14] G. te Velde and E. J. Baerends, Phys. Rev. B **44**, 7888 (1991).
[15] G. te Velde and E. J. Baerends, Chem. Phys. **177**, 399 (1993).
[16] G. J. Kroes, Prog. Surf. Sci. **60**, 1 (1999).
[17] A. Gross, Surf. Sci. Rep. **32**, 291 (1998).
[18] R. Baer and R. Kosloff, J. Chem. Phys. **106**, 8862 (1997).
[19] R. A. Olsen, G. J. Kroes, O. M. Løvvik, and E. J. Baerends, J. Chem. Phys. **107**, 10652 (1997).
[20] Z. S. Wang, G. R. Darling, and S. Holloway, Phys. Rev. Lett. **87**, 226102 (2001).
[21] H. F. Busnengo, W. Dong, P. Sautet, and A. Salin, Phys. Rev. Lett. **87**, 127601 (2001).
[22] J. Dai and J. C. Light, J. Chem. Phys. **107**, 1676 (1997).
[23] E. Pijper, Ph.D. thesis (unpublished).
[24] J. C. Light, I. P. Hamilton, and J. V. Lill, J. Chem. Phys. **82**, 1400 (1985).
[25] M. D. Feit, J. J. A. Fleck, and A. Steiger, J. Comput. Phys. **47**, 412 (1982).
[26] D. Kosloff and R. Kosloff, J. Comput. Phys. **52**, 35 (1983).
[27] G. C. Corey and D. Lemoine, J. Chem. Phys. **97**, 4115 (1992).
[28] D. Lemoine, J. Chem. Phys. **101**, 10526 (1994).
[29] A. Vibók and G. G. Balint-Kurti, J. Phys. Chem. **96**, 8712 (1992).
[30] G. G. Balint-Kurti, R. N. Dixon, and C. C. Marston, J. Chem. Soc., Faraday Trans. **86**, 1741 (1990).
[31] C. C. Marston, G. G. Balint-Kurti, and R. N. Dixon, Theor. Chim. Acta **79**, 313 (1991).
[32] G. G. Balint-Kurti, R. N. Dixon, and C. C. Marston, Int. Rev. Phys. Chem. **11**, 317 (1992).
[33] R. A. Olsen, G. J. Kroes, and E. J. Baerends, J. Chem. Phys. **11**, 11155 (1999).
[34] P. H. T. Philipsen, E. van Lenthe, J. G. Snijders, and E. J. Baerends, Phys. Rev. B **56**, 13556 (1997).
[35] R. A. Olsen, H. F. Busnengo, A. Salin, M. F. Somers, G. J. Kroes, and E. J. Baerends, J. Chem. Phys. **116**, 3841 (2002).
[36] D. Neuhauser and M. Baer, J. Chem. Phys. **91**, 4651 (1989).
[37] J. Sheng and J. Z. H. Zhang, J. Chem. Phys. **97**, 6784 (1992).
[38] J. Sheng and J. Z. H. Zhang, J. Chem. Phys. **99**, 1373 (1993).
[39] R. C. Mowrey, J. Chem. Phys. **99**, 7049 (1993).
[40] G. R. Darling and S. Holloway, Surf. Sci. **304**, L461 (1994).
[41] G. R. Darling and S. Holloway, J. Chem. Phys. **101**, 3268 (1994).
[42] J. Dai, J. Sheng, and J. Z. H. Zhang, J. Chem. Phys. **101**, 1555 (1994).
[43] J. Dai and J. Z. H. Zhang, J. Chem. Phys. **102**, 6280 (1995).
[44] R. C. Mowrey, G. J. Kroes, G. Wiesenekker, and E. J. Baerends, J. Chem. Phys. **106**, 4248 (1997).
[45] R. C. Mowrey, G. J. Kroes, G. Wiesenekker, and E. J. Baerends, J. Chem. Phys. **110**, 2740 (1999).
[46] A. Gross and M. Scheffler, Prog. Surf. Sci. **53**, 187 (1996).
[47] A. Gross, Surf. Sci. **363**, 1 (1996).
[48] D. A. McCormack, G. J. Kroes, R. A. Olsen, and E. J. Baerends, J. Chem. Phys. **110**, 7008 (1999).
[49] D. A. McCormack, G. J. Kroes, R. A. Olsen, J. A. Groeneveld, J. N. P. van Stralen, E. J. Barends, and R. C. Mowrey, Chem. Phys. Lett. **328**, 317 (2000).
[50] J. Dai and J. C. Light, J. Chem. Phys. **108**, 7816 (1998).
[51] G. J. Kroes, E. J. Baerends, and R. C. Mowrey, J. Chem. Phys. **78**, 3583 (1997).
[52] U. Nielsen, D. Halstead, S. Holloway, and J. K. Nørskov, J. Chem. Phys. **93**, 2879 (1990).
[53] J. E. Müller, Appl. Phys. A: Solids Surf. **A49**, 681 (1989).
[54] J. E. Müller, Surf. Sci. **272**, 45 (1992).
[55] G. R. Darling and S. Holloway, Surf. Sci. **307–309**, 153 (1994).
[56] A. Gross, J. Chem. Phys. **102**, 5045 (1995).
[57] A. Cruz and B. Jackson, J. Chem. Phys. **94**, 5715 (1991).
[58] E. Watts, G. O. Sitz, D. A. McCormack, G. J. Kroes, R. A. Olsen, J. A. Groeneveld, J. N. O. van Stralen, E. J. Baerends, and R. C. Mowrey, J. Chem. Phys. **114**, 495 (2000).
[59] A. Hodgson, P. Samson, A. Wight, and C. Cottrell, Phys. Rev. Lett. **78**, 963 (1997).
[60] P. Samson, A. Nesbitt, B. E. Koel, and A. Hodgson, J. Chem. Phys. **109**, 3255 (1998).
[61] E. Pijper, M. F. Somers, G. J. Kroes, R. A. Olsen, E. J. Baerends, H. F. Busnengo, A. Salin, and D. Lemoine, Chem. Phys. Lett. **347**, 277 (2001).
[62] H. A. Michelsen, C. T. Rettner, and D. J. Auerbach, Surf. Sci. **272**, 65 (1992).
[63] C. T. Rettner, H. A. Michelsen, and D. J. Auerbach, J. Chem. Phys. **102**, 4625 (1995).
[64] M. Gostein and G. O. Sitz, J. Chem. Phys. **106**, 7378 (1997).
[65] A. Gross, S. Wilke, and M. Scheffler, Surf. Sci. **614**, 357 (1996).

Downloaded 27 Mar 2011 to 130.37.129.78. Redistribution subject to AIP license or copyright; see http://jcp.aip.org/about/rights_and_permissions